Nutrigonometry I: using right-angle triangles to quantify nutritional trade-offs in multidimensional performance landscapes

Authors: Juliano Morimoto[1*], Pedro Conceição[2], Christen Mirth[3], Mathieu Lihoreau[4]

Authors' affiliations:

[1] School of Biological Sciences, University of Aberdeen, Zoology Building, Tillydrone Ave, Aberdeen AB24 2TZ

[2] Institute of Mathematics, University of Aberdeen, King's College, Aberdeen AB24 3FX

[3] School of Biological Sciences, Monash, University, Melbourne, Victoria, Australia

[4] Research Center on Animal Cognition (CRCA), Center for Integrative Biology (CBI); CNRS, University Paul Sabatier – Toulouse III, France.

* Correspondence:

Dr Juliano Morimoto

juliano.morimoto@abdn.ac.uk

Running-title: Trigonometry to measure fitness trade-offs

Keywords: Nutritional Geometry, trigonometry, lifespan-reproduction trade-off, fitness maps, *Drosophila melanogaster*

Authors' contributions

JM conceptualised the nutrigronometry model, coded the scripts to conduct the analysis, and wrote the first draft of the manuscript. JM and PC implemented the use of persistence homology. All authors contributed to the revising and editing of the manuscript and approved its submission.

Abstract

Animals regulate their diet in order to maximise the expression of fitness traits that often have different nutritional needs. These nutritional trade-offs have been experimentally uncovered using the Geometric framework for nutrition (GF). However, current analytical methods to measure such responses rely on either visual inspection or complex models applied to multidimensional performance landscapes, making these approaches subjective, or conceptually difficult, computationally expensive, and in some cases inaccurate. This limits our ability to understand how animal nutrition evolved to support life-histories within and between species. Here, we introduce a simple trigonometric model to measure nutritional trade-offs in multidimensional landscapes ('Nutrigonometry'). Nutrigonometry is both conceptually and computationally easier than current approaches, as it harnesses the trigonometric relationships of right-angle triangles instead of vector calculations. Using landmark GF datasets, we first show how polynomial (Bayesian) regressions can be used for precise and accurate predictions of peaks and valleys in performance landscapes, irrespective of the underlying structure of the data (i.e., individual food intakes *vs* fixed diet ratios). Using trigonometric relationships, we then identified the known nutritional trade-off between lifespan and reproductive rate both in terms of nutrient balance and concentration. Nutrigonometry enables a fast, reliable and reproducible quantification of nutritional trade-offs in multidimensional performance landscapes, thereby broadening the potential for future developments in comparative research on the evolution of animal nutrition.

Introduction

Animals often require different nutrient blends to maximize concurrent life-history traits, creating the potential for a conflict between nutrient allocation (Simpson and Raubenheimer 2012; Raubenheimer and Simpson 2020). When the optimum nutrition for several traits cannot be achieved simultaneously, a compromise in feeding decisions must exist in order to support the expression of one trait over another ('nutritional trade-off') (Lee et al. 2008; Maklakov et al. 2008). Previous research has identified nutritional trade-offs between lifespan and reproduction or between immunity and reproduction across many different taxa including *D. melanogaster* (Lee et al. 2008; Ponton et al. 2015), tephritid fruit flies (Fanson and Taylor 2012; Fanson et al. 2012), crickets (Maklakov et al. 2008; Rapkin et al. 2018; Guo et al. 2021; Treidel et al. 2021) and mice (Solon-Biet et al. 2014) [see also reviews by (Ponton et al. 2011; Schwenke et al. 2016)]. Even traits related to different aspects of the same life-history can vary in nutritional requirements during the lifetime of an animal, as seen for pre- and post-mating traits related to reproduction of many insect species such as sperm number and viability (Bunning et al. 2015), fertilization success across sperm competitive contexts (Morimoto and Wigby 2016), cuticular hydrocarbons, courtship song and sperm viability (Ng et al. 2018) as well as size and numbers of eupyrene and apyrene sperms (Gage and Cook 1994). Thus, nutritional trade-offs are likely ubiquitous and impose significant constraints on the feeding behaviour of individuals.

Measuring nutritional trade-offs can be challenging because of the interactive effects of nutrient ratios and concentrations on the expression of life-histories (Stearns 1992; Roff 2002; Hunt et al. 2004; Simpson and Raubenheimer 2012). In the last decades, however, a method known as Geometric Framework of Nutrition (GF) has emerged as a powerful unifying framework capable of disentangling the multidimensional effects of nutrients (both

ratios and concentrations) on life-history traits and fitness (Simpson and Raubenheimer 1993*a*). The GF has been applied to a diverse range of nutritional studies across species such as flies (Lee et al. 2008; Reddiex et al. 2013; Jensen et al. 2015; Ponton et al. 2015; Morimoto and Wigby 2016; Kutz et al. 2019) (Fanson and Taylor 2012; Fanson et al. 2012) (Barragan-Fonseca et al. 2018, 2021), crickets (Ng et al. 2018) (Rapkin et al. 2018) (Maklakov et al. 2008), cockroaches (Bunning et al. 2015), domestic cats and dogs (Hewson-Hughes et al. 2011, 2013), and mice (Solon-Biet et al. 2014; Morimoto et al. 2019), being paramount for advancing our understanding of complex physiological and behavioural processes across ecological environments and even human health (Simpson et al. 2017). As a result, developing a simple, intuitive, and accurate quantitative method for quantifying nutritional trade-offs has become a key issue for comparative nutrition, which will allow new avenues of research for insights into the evolution of physiological and behavioural modulation of nutritional responses (Morimoto and Lihoreau 2020).

Recent initiatives have been made but these are complex to navigate and therefore studies continue to be published with visual inspection or with inaccurate methods to quantify the strength of nutritional trade-offs in GF landscapes [e.g., (Polak et al. 2017; Ng et al. 2018, 2019; Kutz et al. 2019; Ma et al. 2020; Barragan-Fonseca et al. 2021)]. Why is it so difficult to measure nutritional trade-offs in GF multidimensional fitness landscapes? The fundamental limitation in all models so far is identifying and delimitating the region of interest (i.e., peaks and, to a lesser extent, valleys) for comparisons of distances between peaks of different traits (or same trait between species). For instance, (Rapkin et al. 2018) proposed the use of regression slopes (rather than the coordinates of the optimum) nutrients onto the fitness trait *i* as coordinates of a vector $\vec{v}_i$. From this, the angle θ' between vectors $\vec{v}_i$ and $\vec{v}_j$ for traits *i* and *j*, respectively, can be calculated as the estimate of the strength of the

nutritional trade-off. However, in this approach, the domain of each vector coordinate is all real numbers $\mathbb{R}$ even though the domain of the fitness landscape is constrained to all positive real numbers $\mathbb{R}^+$. Consequently, this violates the domain constraints of the nutritional space upon which GF is performed, which in turn result in overestimation of the strength of nutritional trade-offs (Morimoto and Lihoreau 2019). To address this limitation, we proposed to use the coordinates of the peak (or valley) from the nutritional space as vector coordinates for the position vector $\vec{v}_i$, from which the angle θ between position vectors $\vec{v}_i$ and $\vec{v}_j$ for traits *i* and *j*, respectively, can be estimated as measure of the strength of the nutritional trade-off. This overcomes the violation of domains between vector coordinates and the nutritional space [in (Rapkin et al. 2018)] and therefore ensures that the estimate of θ is calculated in the same domain of the GF fitness landscapes. However, this Vector of Positions approach relies on the peak estimates from a SVM machine learning model which is computationally expensive particularly in *n* dimensions, where n > 3, and sensitive to the characteristics of the input data (e.g., if the data contains food intakes as in (Lee et al. 2008; House et al. 2015; Jensen et al. 2015; Morimoto and Lihoreau 2019) or a grid of fixed diet ratios as in (Kutz et al. 2019)], identifying local as well as global peaks that introduce noise into the analysis (shown here). Albeit useful, the Vector of Positions approach can be cumbersome to implement across different datasets, computationally expensive to obtain estimates of peaks (or valleys), and as a result can generate inaccurate estimates of the strength of nutritional trade-offs. Thus, to date, there are no proposed solutions that address the above limitations, which creates a significant bottleneck in studies of nutrition that limits the multidimensional power of the GF framework.

Here, we address the limitations of current models by proposing a simpler framework (Nutrigonometry) upon which the strength of nutritional trade-offs can be calculated in 3D

fitness landscapes, irrespective of the structure of the nutritional data to analyze. Using landmark GF datasets, we first investigated the performance of different 'off-the-shelf' machine learning models in predicting the peak in the fitness landscapes, in order to find the most accurate and computationally inexpensive model. We achieved this by integrating several measurements of predictive error, variance in predicted peak area, and topological characteristics of the predicted peak region. Next, we used simple trigonometric functions and relationships to estimate the strength of nutritional trade-offs both in terms of nutrient balance as well as nutrient concentration, or both. Our approach opens new avenues of research in multidimensional nutrition, and allows for physiological and comparative studies to be performed in a consistent and reproducible way from which insights onto the evolution of animal nutrition can be gained across the tree of life.

Material and Methods

Nutrigonometry

Studies using GF define the food components (typically macro-nutrients) that will be investigated, which together compose the 'nutritional space'. For example, in studies where protein and carbohydrate effects are investigated, there is a 2D nutritional space (one dimension for each nutrient) onto which the performance landscape of the trait is mapped. This rationale can be extended to *n* number of nutrients (Simpson and Raubenheimer 1993*b*), albeit to date, studies with two nutrients are the most common (Morimoto and Lihoreau 2020). If we consider this 2D nutritional space as a rectangular space in which an infinite number of nutritional rails (i.e., imaginary lines that pass through the origin with arbitrary positive slope) exist that divides the space in right-angle triangles, then it is possible to use simple trigonometric functions to estimate the angle α_i and the hypothenuse of the triangle, for all fitness traits mapped onto the nutritional space. The angle α_i is the angle of the

nutritional rail, relative from the x-axis, that passes through the peak in the landscape for the trait *i*, and the hypothenuse h_i of the triangle shows how far from the origin the peak in the landscape sits for the trait *i* (Fig 1a). α_i and h_i can be calculated using Pythagorean theorem and the relationship between the angle and the sides of right-angle triangles (i.e., sines and cosines), as shown in Fig 1a.

Once α_i are known, we can estimate the angle θ [as in (Morimoto and Lihoreau 2019)] which is the difference in the angle between nutritional rails that maximize two traits, *i* and *j*, and provides a measure of the strength of the nutritional trade-off that exists between traits *i* and *j* (Fig 1b). The larger the angle $\theta_{i,j}$, the strongest the nutritional trade-off in terms of nutrient balance (and potentially nutritional compromise) between traits. Likewise, we can compare the difference $h_{i,j}$ in the estimates of the hypothenuse h_j and h_i to quantify nutritional trade-offs in relation to nutrient concentration (Fig 1b). These metrics allowed us to disentangle the following scenarios in which nutritional trade-off can occur:

(I) When $\theta_{i,j}$ is large but $h_{i,j}$ is small ('Strong nutritional trade-off in terms of nutrient balance')

(II) When $\theta_{i,j}$ is small but $h_{i,j}$ is large ('Strong nutritional trade-off in terms of nutrient concentration'),

(III) When $\theta_{i,j}$ and $h_{i,j}$ are large ('Strong nutritional trade-off in terms of both nutrient balance and concentration')

(IV) When $\theta_{i,j}$ and $h_{i,j}$ are small ('Weak or no nutritional trade-off') (Fig 1c).

Here when applying this model for empirical datasets (see below), inferences on the strength of nutritional trade-offs were made using confidence intervals for $h_{i,j}$ and $\theta_{i,j}$, whereby nutritional trade-offs were stronger when confidence intervals did not overlap zero and the

174 magnitude of the difference was large. Estimates are presented in the units of the nutrient
175 space in which the data was collected (e.g., mg), while angles are presented in degrees.
176 Confidence intervals for both $h_{i,j}$ and $\theta_{i,j}$ were calculated using the significance threshold of
177 0.05 and the quartiles of a *t*-distribution. All analyses and plots were done in R version 3.6.2
178 (R Core Team 2019).
179
180 ***Predicting peak (or valley) location and size***
181 As with previous approaches, the model presented here depends on accurate estimates of the
182 coordinates for the peak in the multidimensional performance landscape. Without this,
183 estimates of $h_{i,j}$ and θ are inaccurate which in turn affects the ability of the model to estimate
184 the strength of nutritional trade-offs. To overcome this, the basic algorithms underpinning the
185 identification of peak regions in multidimensional fitness landscapes were designed as
186 following:
187 1) Empirical data was split into training (75%) and test (25%) datasets;
188 2) A machine learning model was fitted to the training set using 10-fold cross-validation,
189 with the fitness trait as dependent variable and the nutrient intakes (or fixed ratios) as
190 independent variables. The model included main and interactive effects of protein and
191 carbohydrate, as well as quadratic effects of each nutrient (for non-linear
192 relationships);
193 3) The model's predictive performance was evaluated with root-mean-square-error
194 (RMSE) with respect to the observed values of the test dataset;
195 4) A set of 500 random points corresponding to (protein, carbohydrate) coordinates were
196 generated covering the nutritional space, and the model of step 2 was used to predict
197 the value of the fitness value for each point;

5) A quantile threshold was used to crop the data to the specific region of interest. For instance, for peaks in the nutritional landscape, the default value used throughout this study was set to 0.95 (i.e., the highest 5% predicted fitness values are subset, from which coordinates of protein and carbohydrate are used).
6) Steps 4-5 were repeated 100 times.

We then made statistical inferences on peak area from 95% confidence intervals using the 'ci' function of the 'Rmisc' package (Hope et al. 2013) whereby we resampled with replacement the selected random points obtained from steps 5 and 6 above. To test the performance of nutrigonometry in estimating nutritional trade-offs, we used the most commonly used models to test relationships between traits in behavioral ecology (e.g., general linear model), machine learning models used in regression models in ecology and evolution [e.g., Random Forest, (Rabinovich 2021)], as well as models that have been specifically used to analyse multidimensional performance landscapes in GF studies (e.g., SVM, GAMs) (Ponton et al. 2015; Morimoto and Lihoreau 2019). In particular, we tested the performance of Bayesian linear regression (Bayes), general linear regression (LM), k-nearest neighbors (KNN), Gradient boost (GBoost), random forest (RF), support vector machine (SVM) with radial basis function as well as generalized additive models (GAMs) with both smooth term or tensor product term. With the exception of GAMs that were fitted using the 'mgcv' package (Wood and Wood 2015), all other models were fitted using the 'tidymodels' package of the tidyverse (Wickham et al. 2019). For the Bayesian regression, we used the flexible Cauchy prior from the 'rstanarm' package for all analysis (Goodrich et al. 2020). Fitness landscapes were estimated using the 'Tps' function of the 'fields' package (Nychka et al. 2017). All plots were done using the 'ggplot2' package (Wickham 2016). All models were fitted to a training set (75% of the data) and model performance (i.e., RMSE) was calculated from the performance of the models in the remaining test dataset (25%).

223

224 ***Goodness-of-estimate of the models***

225 In addition to RSME, we estimated the area (in squared units in which the data is collected)
226 of the polygon delimited by the estimated predicted peak region ('Area') and the horizontal
227 (protein) and vertical (carbohydrate) spread of the datapoints of the predicted peak region
228 ('Nutrient spread') as proxies of the goodness-of-estimate of the models (Fig 1d). The smaller
229 the RMSE, the better is the model in predicting the fitness value of the peak region (the z-
230 axis). Furthermore, the smaller the area and nutrient spread, the more compact the prediction
231 of the peak region in the nutritional space. Note that RMSE values do not interfere with
232 accuracy of estimates of $h_{i,j}$ and θ, and thus the estimates of nutritional trade-offs, because
233 the z-axis is not used in the calculation of angles and hypothenuses (Fig 1d). A model can
234 have high RMSE and still be the best predictive model as long as the predicted peak correctly
235 matches with the observed peak in the landscape.

236

237 ***Topological structure of the estimated peak***

238 Even in cases where area and nutrient spread of the predicted peak region are small, it is
239 important to have evenly-spaced datapoints within the predicted peak region. This is because
240 predictions of regions which contain holes can lead to mis-estimation of the strength of
241 nutritional trade-offs by potentially adding noise to the set of protein and carbohydrate
242 coordinates used to calculate $h_{i,j}$ and θ. We measured the topological structure of the
243 predicted peak region using the concept of persistence homology (PH), which in simple
244 terms, allows us to investigate the overall structural organisation of the data [see Text S1 and
245 (Zomorodian and Carlsson 2005; Weinberger 2011) for details of the concept] (Fig 1d). PH
246 was estimated using the 'TDAstats' package (Wadhwa et al. 2018). Together, the estimates of

RMSE, area, nutrient spread, and PH provided a comprehensive suite of metrics to assess the quality of model predictions for the peak region in fitness landscapes.

Datasets used for model application

We demonstrate the applications of the Nutrigonometry framework using two datasets, which vary in structure. The first dataset is a landmark dataset which contains *Drosophila melanogaster* individual adult nutrient intake as well as the consequences of nutrient intake to lifespan and reproduction (Lee et al. 2008). This dataset was previously used to test the Vector of Position approach and therefore has important benchmark status in the field (Morimoto and Lihoreau 2019). We also investigate the effect of data structure on Nutrigonometry estimates of peak and valley regions. In GF, data can be divided into two structures: intake data and fixed ratio data. Intake data is ideal in GF studies because it allows for exploration of *realized* nutritional effects, that is, nutritional effects exerted upon traits given by the amount of nutrient eaten (Simpson and Raubenheimer 1993*b*). However, collecting intake data can be cumbersome or challenging, and recent approaches have adapted GF experiments to draw landscapes of traits based on the fixed ratio of the nutrients in the diets (Kutz et al. 2019). To date, however, we still do not know how this adaptation influence estimates of nutritional trade-offs in multidimensional performance landscapes. Here, to test whether the structure of the data is important for model predictions, we used Lee et al., (2008) dataset with individual intakes ('intakes') as well as with fixed ratios ('fixed'). Using this data and for the purpose of the demonstration of Nutrigonometry, we estimated the nutritional trade-off between lifespan and reproductive rate which are known to trade-off in this species. We also used a second dataset from (Kutz et al. 2019), which studied how temperature modulates nutritional responses of larval development and adult fitness in *D. melanogaster*, as an additional proof-of-application of our model in fixed ratio datasets (see

Fig S1). Lastly, we demonstrated how the best performing models in our peak analysis can be used to predict valley regions (Fig S2 and Fig S3).

Comparison with intake target

Drosophila melanogaster balance their nutrient intake to a P:C ratio of 1:4 when given the possibility to self-select multiple nutritionally complementary foods (Lee et al. 2008). We then used the peak predictions of the Nutrigonometry framework to test whether the observed P:C ratios that maximized lifespan and reproductive rates coincided with the P:C ratio of 1:4 reached by flies in choice situations. To achieve this, we calculated the 95% confidence interval as described for the peak area but in this case, for the P:C ratio of each trait. Whenever the confidence interval overlapped 1:4, we inferred that the estimate of peak ratio did not statistically differ from the intake target of 1:4.

Results

Simple (Bayesian) linear regressions outshine machine learning models when predicting peak region in multidimensional landscapes

All models generated predictions of peak region in nutritional landscapes irrespective of data structure although the accuracy and topology of the predicted regions varied (Fig 2 and Fig 3). In general, GAMs with tensor product and smooth function as well as Bayes and LM linear models generated peak predictions for both lifespan and reproductive rate that were significantly more accurate (narrower in area) than other models when the structure of the data was composed of food intakes (Fig 2, Table S1 and Table S2). When the data structure changed to fixed ratios, LM, GAM with tensor product, Bayes, and KNN predicted peaks with smaller area for lifespan and all but KNN perform within similar scales for the peak prediction of reproductive rate (Fig 2, Table S1 and Table S2). In comparison, GAM smooth

297 did not perform well in predicting peak region that was homogenous and accurate to the
298 performance landscape, particularly when the data structure was fixed ratio. The performance
299 of the models was independent of patterns in the estimates of RMSE and nutrient spread
300 which showed no clear pattern of performance with the exception of LM and Bayes that
301 displayed consistently lower spread when the structure of the data were intakes (Fig 3 and Fig
302 4; Table S2). Interestingly, machine learning models consistently underperformed, predicting
303 peak regions that were wider and less accurate and homogenous (Fig 2 and 3, Table S1 and
304 S2). The underlying reason for this is unclear, but similar patterns were observed when
305 predicting the peak region of (Kutz et al. 2019) dataset (see Fig S1 and Table S3). Bayes,
306 GAMs (both smooth and tensor product) and LM also performed well when predicting valley
307 regions (see Fig S2 and S3). These results indicate that simple (Bayesian) linear regression
308 provide consistently the best models to estimate the region of the peak of fitness landscapes
309 irrespective of the structure of the data, and that GAMs with tensor product (and to a smaller
310 extent, smooth function) can be used when the data are individual intakes.
311
312 ***Better models lead to accurate estimates of known nutritional trade-offs in***
313 ***multidimensional landscapes***
314 GAMs (both smooth and tensor product), Bayes, LM, and KNN models were the only models
315 that correctly identified the nutritional trade-off measured by θ between lifespan and
316 reproductive rate for data with individual intakes (Table 1). Given the variability in the area,
317 spread, and topology of the predicted region, estimates of $h_{i,j}$ and θ were more accurate
318 (narrower confidence intervals) for GAMs (smooth and tenor product), Bayes and LM
319 compared with KNN. GAMs, Bayes and LM were the only ones that identified a trade-off on
320 the hypothenuse estimate $h_{i,j}$ for data of individual intakes, while KNN was the only model
321 that identified this trade-off in data with fixed ratio. GAM smooth was the only model that

failed to identify this trade-off when the data was composed of fixed ratios (Table 1). Thus, overall, simpler models are more suitable to generate peak predictions that accurately describe nutritional trade-offs in multidimensional performance landscapes for data of different structures.

Comparing trait optimum with intake target

We then used the estimated peak regions for lifespan and reproductive rate (both individual intake and fixed ratio data structures) to estimate the optimum P:C ratio that maximises each trait as well as whether or not these optima coincided with the P:C ratio obtained when individuals are allowed to balance their diet (i.e., 1:4). All models predicted a significantly lower P:C ratio for the optimum that maximizes reproductive rate relative to lifespan as expected from the original visual comparison of landscapes (around 1:2 for reproductive rate and >1:9 for lifespan) (Table 2). However, none of the estimates overlapped 1:4, suggesting that *D. melanogaster* females likely have to compromise the nutrient intake to maximise either lifespan or reproductive rate, but not both simultaneously.

Discussion

We proposed a new simple analytical framework to analyse nutritional trade-offs in multidimensional fitness landscapes. Nutrigonometry uses trigonometric relationships from right-angle triangles to identify and compare peaks (or valleys) in 3D fitness landscapes between traits. Using landmark GF datasets with different structures, we demonstrated the accuracy and performance of standard (machine learning) models in finding the peak regions in these multidimensional landscapes and subsequently quantifying the strength of nutritional trade-offs between traits. As with the Vector of Positions approach (Morimoto and Lihoreau 2019), the Nutrigonometry strictly considers coordinates in the real positive region of the

nutrient space, whereby the true separation between key regions (peaks and valleys) are quantified within the correct domain in which the fitness landscapes exist. However, contrary to previous methods (Rapkin et al. 2018; Morimoto and Lihoreau 2019), the Nutrigonometry does not rely on vector calculations but instead harnesses the trigonometric relationships of right-angle triangles to estimate nutritional trade-offs. This is a major advance of the model as it considerably simplifies the framework both in conceptual and computational terms. Nutrigonometry thus significantly advances our ability to generate reliable and reproducible estimates of nutritional trade-offs within and between species, facilitating quantitative (comparative studies) of animal nutrition.

Multidimensional studies of nutrition through the GF have been increasingly used to gain insight into animal and human nutrition (Lee et al. 2008; Behmer 2009; Felton et al. 2009; Simpson and Raubenheimer 2012; Hewson-Hughes et al. 2013; Gosby et al. 2014; Solon-Biet et al. 2014). Likewise, the complexity of the applications has also increased, ranging from studies with few nutrients (e.g., protein and carbohydrates, salts) through to high-dimensional studies investigating individual fatty acids and amino acids (Simpson et al. 2006; Grandison et al. 2009; Arien et al. 2015; Arganda et al. 2017; Piper et al. 2017). This means that analytical frameworks that are simple and robust must be developed to support the development of the field. Nutrigonometry provides such foundation, by demonstrating the best approach to investigate nutritional trade-offs in 3D fitness landscapes. Because Nutrigonometry uses trigonometric relationships of right-angle triangle, it is applicable to *n* dimensions. However, given the often counter-intuitive geometrical effects of high dimensionality [e.g., (Milman 1998; Watanabe 2021)], such expansion to higher dimensions requires further investigation as the topic of future developments. Nevertheless, given the broad use of 3D fitness landscapes in GF studies (Morimoto and Lihoreau 2020),

372 Nutrigonometry readily enables important quantifications of nutritional trade-offs that were
373 otherwise absent or cumbersome to produce. For instance, using a range of models,
374 Nutrigonometry uses right-angle triangles to compare the ratio of nutrients that maximise
375 lifespan and reproductive rate along with the strength of nutritional trade-offs between these
376 traits in a landmark paper in the field (Lee et al. 2008). Moreover, Nutrigonometry is capable
377 of comparing the nutrient ratio which maximises lifespan and reproductive rate with the
378 nutrient ratio that is balanced by individuals when given a choice, providing important
379 insights into the dietary choices underpinning nutritional compromises. Such quantification
380 can bring new fundamental insights into our understanding of nutritional trade-offs such as
381 strength and the direction of the trade-offs (e.g. nutrient balance vs concentration, see Fig. 1),
382 as well as how much animals actually resolve these trade-offs when they have the opportunity
383 to do so and whether, for instance, they favour one trait of another (distance between optimal
384 trade-off and observed nutrient intake target, see Table 2).
385
386 An important trend in the field of multidimensional nutrition is the study of nutritional effects
387 across physiological pathways and across levels of biological organization (Lihoreau et al.
388 2014; Simpson et al. 2015). These studies generate multiple 3D landscapes that are often
389 compared visually, without rigorous analytical methods to measure nutritional trade-offs. For
390 example, eleven 3D-landscapes of the expression of genes involved in the Insulin/IGF
391 pathway were visually compared to provide insights into how a key endocrine pathway is
392 regulated based on nutrient intake, and how gene expression can underlie expression of life-
393 histories (Post and Tatar 2016; McDonald et al. 2021). Likewise, twelve 3D-landscapes with
394 gut microbial diversity or abundance were visually compared to better understand how
395 nutrient composition can modulate host-microbe interactions (Ng et al. 2019). Similar visual
396 comparisons have been made to understand the effects of nutrition on host-endosymbiont

relationship (Ponton et al. 2015). The analytical framework proposed here will allow researchers to move beyond visual comparisons to quantitatively assess how landscapes differ using a rigorous and reproducible framework. As a result, Nutrigonometry yields considerable advances to the status quo in the field, enabling a deeper understanding of the role of nutrition in host-microbial interactions as well as animal physiology, behaviour and ecology.

Acknowledgements

ML receives support from the CNRS, the French Research Agency (ANR 3DNaviBee: ANR-19-CE37-0024), the European Regional Development Fund (FEDER ECONECT: MP0021763), and the European Research Council (ERC-CoG BEE-MOVE: GA101002644).

Data accessibility

Kutz et al. data is available here: doi.org/10.26180/5cfe1ddaaafac. Lee et al. dataset is available in Dryad: doi:10.5061/dryad.tp7519s. R script with functions for the implementation of the Nutrigonometry framework is available in the Supplementary Materials.

References

Arganda, S., S. Bouchebti, S. Bazazi, S. Le Hesran, C. Puga, G. Latil, S. J. Simpson, et al. 2017. Parsing the life-shortening effects of dietary protein: effects of individual amino acids. Proceedings of the Royal Society B: Biological Sciences 284:20162052.

Arien, Y., A. Dag, S. Zarchin, T. Masci, and S. Shafir. 2015. Omega-3 deficiency impairs honey bee learning. Proceedings of the National Academy of Sciences of the United States of America 112:15761–15766.

Barragan-Fonseca, K. B., M. Dicke, and J. J. A. van Loon. 2018. Influence of larval density and dietary nutrient concentration on performance, body protein, and fat contents of black soldier fly larvae (*Hermetia illucens*). Entomologia Experimentalis et Applicata 166:761–770.

Barragan-Fonseca, K. B., G. Gort, M. Dicke, and J. J. A. van Loon. 2021. Nutritional plasticity of the black soldier fly (H*ermetia illucens*) in response to artificial diets varying in protein and carbohydrate concentrations. Journal of Insects as Food and Feed 7:51–61.

Behmer, S. T. 2009. Insect herbivore nutrient regulation. Annual Review of Entomology 54:165–187.

Bunning, H., J. Rapkin, L. Belcher, C. R. Archer, K. Jensen, and J. Hunt. 2015. Protein and carbohydrate intake influence sperm number and fertility in male cockroaches, but not sperm viability. Proceedings of the Royal Society B: Biological Sciences 282:20142144.

del Castillo, E., P. Chen, A. Meyers, J. Hunt, and J. Rapkin. 2020. Confidence regions for the location of response surface optima: the R package OptimaRegion. Communications in Statistics-Simulation and Computation 1–21.

del Castillo, E., J. Hunt, and J. Rapkin. 2016. OptimaRegion: confidence regions for Optima. R package version 0.2.

Fanson, B. G., and P. W. Taylor. 2012. Protein:carbohydrate ratios explain life span patterns found in Queensland fruit fly on diets varying in yeast:sugar ratios. Age (Dordr) 34:1361–1368.

Fanson, B. G., S. Yap, and P. W. Taylor. 2012. Geometry of compensatory feeding and water consumption in *Drosophila melanogaster*. Journal of Experimental Biology 215:766–773.

Felton, A. M., A. Felton, D. Raubenheimer, S. J. Simpson, W. J. Foley, J. T. Wood, I. R. Wallis, et al. 2009. Protein content of diets dictates the daily energy intake of a free-ranging primate. Behavioral Ecology. 20:685-690

447 Gage, M. J. G., and P. A. Cook. 1994. Sperm size or numbers - Effects of nutritional stress
448 upon eupyrene and apyrene sperm production strategies in the moth *Plodia-Interpunctella*
449 (Lepidoptera, Pyralidae). Functional Ecology 8:594–599.
450 Goodrich, B., J. Gabry, I. Ali, and S. Brilleman. 2020. rstanarm: Bayesian Applied
451 Regression Modeling via Stan. R Package v. 2.19. 2.
452 Gosby, A. K., A. D. Conigrave, D. Raubenheimer, and S. J. Simpson. 2014. Protein leverage
453 and energy intake. Obesity Reviews 15:183–191.
454 Grandison, R. C., M. D. W. Piper, and L. Partridge. 2009. Amino-acid imbalance explains
455 extension of lifespan by dietary restriction in *Drosophila*. Nature 462:1061–1064.
456 Guo, J., Y. Cui, P. Lin, B. Zhai, Z. Lu, J. W. Chapman, and G. Hu. 2021. Male nutritional
457 status does not impact the reproductive potential of female *Cnaphalocrocis medinalis* moths
458 under conditions of nutrient shortage. Insect Science. doi.org/10.1111/1744-7917.12939
459 Hewson-Hughes, A. K., V. L. Hewson-Hughes, A. Colyer, A. T. Miller, S. J. McGrane, S. R.
460 Hall, R. F. Butterwick, et al. 2013. Geometric analysis of macronutrient selection in breeds of
461 the domestic dog, Canis lupus familiaris. Behavioral Ecology 24:293–304.
462 Hewson-Hughes, A. K., V. L. Hewson-Hughes, A. T. Miller, S. R. Hall, S. J. Simpson, and
463 D. Raubenheimer. 2011. Geometric analysis of macronutrient selection in the adult domestic
464 cat, felis catus. Journal of Experimental Biology 214:1039–1041.
465 Hope, R. M., M. R. M. Hope, and R. Collate'CI. 2013. Package 'Rmisc.' group 101:2.
466 House, C. M., K. Jensen, J. Rapkin, S. Lane, K. Okada, D. J. Hosken, and J. Hunt. 2015.
467 Macronutrient balance mediates the growth of sexually selected weapons but not genitalia in
468 male broad□horned beetles. Functional Ecology. 30:769-779
469 Hunt, J., R. Brooks, M. D. Jennions, M. J. Smith, C. L. Bentsen, and L. F. Bussiere. 2004.
470 High-quality male field crickets invest heavily in sexual display but die young. Nature
471 432:1024–1027.

Jensen, K., C. McClure, N. K. Priest, and J. Hunt. 2015. Sex-specific effects of protein and carbohydrate intake on reproduction but not lifespan in *Drosophila melanogaster*. Aging Cell 14:605-615

Kutz, T. C., C. M. Sgrò, and C. K. Mirth. 2019. Interacting with change: Diet mediates how larvae respond to their thermal environment. Functional Ecology 33:1940–1951.

Lee, K. P., S. J. Simpson, F. J. Clissold, R. Brooks, J. W. Ballard, P. W. Taylor, N. Soran, et al. 2008. Lifespan and reproduction in Drosophila: New insights from nutritional geometry. Proceedings of the National Academy of Sciences of the United States of America 105:2498–2503.

Lihoreau, M., J. Buhl, M. A. Charleston, G. A. Sword, D. Raubenheimer, and S. J. Simpson. 2014. Modelling nutrition across organizational levels: from individuals to superorganisms. Journal of Insect Physiology 69:2–11.

Ma, C., C. K. Mirth, M. D. Hall, and M. D. W. Piper. 2020. Amino acid quality modifies the quantitative availability of protein for reproduction in *Drosophila melanogaster*. Journal of insect physiology 104050.

Maklakov, A. A., S. J. Simpson, F. Zajitschek, M. D. Hall, J. Dessmann, F. Clissold, D. Raubenheimer, et al. 2008. Sex-specific fitness effects of nutrient intake on reproduction and lifespan. Current Biology 18:1062–1066.

McDonald, J. M. C., P. Nabili, L. Thorsen, S. Jeon, and A. W. Shingleton. 2021. Sex-specific plasticity and the nutritional geometry of insulin-signaling gene expression in *Drosophila melanogaster*. EvoDevo 12:1–17.

Milman, V. 1998. Surprising geometric phenomena in high-dimensional convexity theory. Pages 73–91 *in*European Congress of Mathematics. Springer.

Morimoto, J., and M. Lihoreau. 2019. Quantifying nutritional trade-offs across multidimensional performance landscapes. The American Naturalist 193:E168–E181.

———. 2020. Open data for open questions in comparative nutrition. Insects 11:236.

Morimoto, J., A. Senior, K. Ruiz, J. A. Wali, T. Pulpitel, S. M. Solon-Biet, V. C. Cogger, et al. 2019. Sucrose and starch intake contribute to reduced alveolar bone height in a rodent model of naturally occurring periodontitis. PLoS ONE 14.

Morimoto, J., and S. Wigby. 2016. Differential effects of male nutrient balance on pre-and post-copulatory traits, and consequences for female reproduction in *Drosophila melanogaster*. Scientific Reports 6.

Ng, S. H., S. J. Simpson, and L. W. Simmons. 2018. Macronutrients and micronutrients drive trade□offs between male pre□and postmating sexual traits. Functional Ecology 32:2380–2394.

Ng, S. H., M. Stat, M. Bunce, S. J. Simpson, and L. W. Simmons. 2019. Protein and carbohydrate intakes alter gut microbial community structure in crickets: a Geometric Framework approach. FEMS Microbiology Ecology 95.

Nychka, D., F. Reinhard, J. Paige, and S. Sain. 2017. fields: Tools for spatial data. R package 9.9.

Piper, M. D. W., G. A. Soultoukis, E. Blanc, A. Mesaros, S. L. Herbert, P. Juricic, X. He, et al. 2017. Matching dietary amino acid balance to the in silico-translated exome optimizes growth and reproduction without cost to lifespan. Cell metabolism 25:610–621.

Polak, M., L. W. Simmons, J. B. Benoit, K. Ruohonen, S. J. Simpson, and S. M. Solon-Biet. 2017. Nutritional geometry of paternal effects on embryo mortality. Proceedings of the Royal Society B: Biological Sciences 284:20171492.

Ponton, F., K. Wilson, S. C. Cotter, D. Raubenheimer, and S. J. Simpson. 2011. Nutritional Immunology: A Multi-Dimensional Approach. PLoS Pathogens 7:e1002223.

Ponton, F., K. Wilson, A. Holmes, D. Raubenheimer, K. L. Robinson, and S. J. Simpson. 2015. Macronutrients mediate the functional relationship between Drosophila and Wolbachia.

Proceedings of the Royal Society B-Biological Sciences 282:20142029.

Post, S., and M. Tatar. 2016. Nutritional geometric profiles of insulin/IGF expression in Drosophila melanogaster. PloS one 11:e0155628.

R Core Team. 2019. R: A language and environment for statistical computing. R Foundation for Statistical Computing.

Rabinovich, J. E. 2021. Morphology, life cycle, environmental factors and fitness-a machine learning analysis in kissing bugs (Hemiptera, Reduviidae, Triatominae). Frontiers in Ecology and Evolution 9:88.

Rapkin, J., K. Jensen, C. R. Archer, C. M. House, S. K. Sakaluk, E. Del Castillo, and J. Hunt. 2018. The geometry of nutrient space-based life-history trade-offs: sex-specific effects of macronutrient intake on the trade-off between encapsulation ability and reproductive effort in decorated crickets. The American Naturalist 191:452–474.

Raubenheimer, D., and S. Simpson. 2020. Eat Like the Animals: What Nature Teaches Us about the Science of Healthy Eating. Houghton Mifflin.

Reddiex, A. J., T. P. Gosden, R. Bonduriansky, and S. F. Chenoweth. 2013. Sex-specific fitness consequences of nutrient intake and the evolvability of diet preferences. The American Naturalist 182:91–102.

Roff, D. A. 2002. Life history evolution (Vol. 7). Sinauer Associates Sunderland.

Schwenke, R. A., B. P. Lazzaro, and M. F. Wolfner. 2016. Reproduction–Immunity Trade-Offs in Insects. Annual Review of Entomology 61:239–256.

Simpson, S. J., F. J. Clissold, M. Lihoreau, F. Ponton, S. M. Wilder, and D. Raubenheimer. 2015. Recent advances in the integrative nutrition of Arthropods. Annual Review of Entomology 60:293–311.

Simpson, S. J., D. G. Le Couteur, D. E. James, J. George, J. E. Gunton, S. M. Solon-Biet, and D. Raubenheimer. 2017. The Geometric Framework for Nutrition as a tool in precision

547 medicine. Nutrition and Healthy Aging 4:217–226.

548 Simpson, S. J., and D. Raubenheimer. 1993*a*. A multi-level analysis of feeding behaviour:

549 the geometry of nutritional decisions. Philosophical Transactions of the Royal Society B-

550 Biological Sciences 342:381–402.

551 Simpson, S. J., and D. Raubenheimer. 1993*b*. A multi-level analysis of feeding behaviour:

552 The geometry of nutritional decisions. Philosophical Transactions of the Royal Society B:

553 Biological Sciences 342:381–402.

554 Simpson, S. J., and D. Raubenheimer. 2012. The Nature of Nutrition: A Unifying Framework

555 From Animal Adaptation to Human Obesity (1st ed.). Princeton university press, Princeton,

556 New Jersey.

557 Simpson, S. J., G. A. Sword, P. D. Lorch, and I. D. Couzin. 2006. Cannibal crickets on a

558 forced march for protein and salt. Proceedings of the National Academy of Sciences of the

559 United States of America 103:4152–4156.

560 Solon-Biet, S. M., A. C. McMahon, J. W. O. Ballard, K. Ruohonen, L. E. Wu, V. C. Cogger,

561 A. Warren, et al. 2014. The ratio of macronutrients, not caloric intake, dictates

562 cardiometabolic health, aging, and longevity in ad libitum-fed mice. Cell Metabolism

563 19:418–430.

564 Stearns, S. C. 1992. The evolution of life histories (Vol. 249). Oxford University Press

565 Oxford.

566 Treidel, L. A., R. M. Clark, M. T. Lopez, and C. M. Williams. 2021. Physiological demands

567 and nutrient intake modulate a trade-off between dispersal and reproduction based on age and

568 sex of field crickets. Journal of Experimental Biology 224:jeb237834.

569 Wadhwa, R. R., D. F. K. Williamson, A. Dhawan, and J. G. Scott. 2018. TDAstats: R

570 pipeline for computing persistent homology in topological data analysis. Journal of Open

571 Source Software 3:860.

572 Watanabe, J. 2021. Detecting (non)parallel evolution in multidimensional spaces: angles,
573 correlations, and eigenanalysis. EcoEvoRxiv 1:25.
574 Weinberger, S. 2011. What is... persistent homology? Notices of the AMS 58:36–39.
575 Wickham, H. 2016. ggplot2: elegant graphics for data analysis. Springer.
576 Wickham, H., M. Averick, J. Bryan, W. Chang, L. D. McGowan, R. François, G. Grolemund,
577 et al. 2019. Welcome to the Tidyverse. Journal of Open Source Software 4:1686.
578 Wood, S., and M. S. Wood. 2015. Package 'mgcv.' R package version 1:29.
579 Zomorodian, A., and G. Carlsson. 2005. Computing Persistent Homology. Discrete &
580 Computational Geometry 33:249–274.
581
582

583 **Table caption**

584
585
586 **Table 1. Nutrigonometry quantification of nutritional trade-offs between lifespan and**
587 **reproduction.** Estimates of $\theta_{i,j}$ (in degrees) and $h_{i,j}$ (in mg) for the nutritional trade-off
588 between lifespan and reproductive rate. Analysis from the data presented in Lee et al. (2008).
589 Confidence intervals overlapping zero implies no difference in the peaks. Magnitude of the
590 estimates indicate the strength of nutritional trade-offs (i.e., larger magnitudes indicate
591 stronger nutritional trade-offs). Note that $\theta_{i,j}$ is bound between 0 and 90 degrees (i.e., 0 and
592 $\frac{\pi}{2}$).
593
594

595 **Table 2. Nutrigonometry estimates of nutritional compromises.** Estimates of optimal
596 intake that maximises lifespan and reproductive rate based on the predicted peak region.
597 Comparison made with the visual peak ratio from Lee et al. (2008). Note that all models
598 show that the estimated peak ratio between traits do not overlap and thus, corroborate the
599 inference of a nutritional trade-off between traits, leading to a nutritional compromise. Note
600 also that all but one model (i.e., GAM smooth for fixed ratio reproductive rate data) predicted
601 peak region ~1:4, which is the ratio that individuals balance when given the ability to balance
602 their diet ('choice'). All other models suggest that a P:C ratio of 1:4 is lower than the ratio
603 needed to maximise lifespan but higher than that for reproductive rate, further supporting the
604 concept of a nutritional compromise.
605
606
607

608

609

610

Figure caption

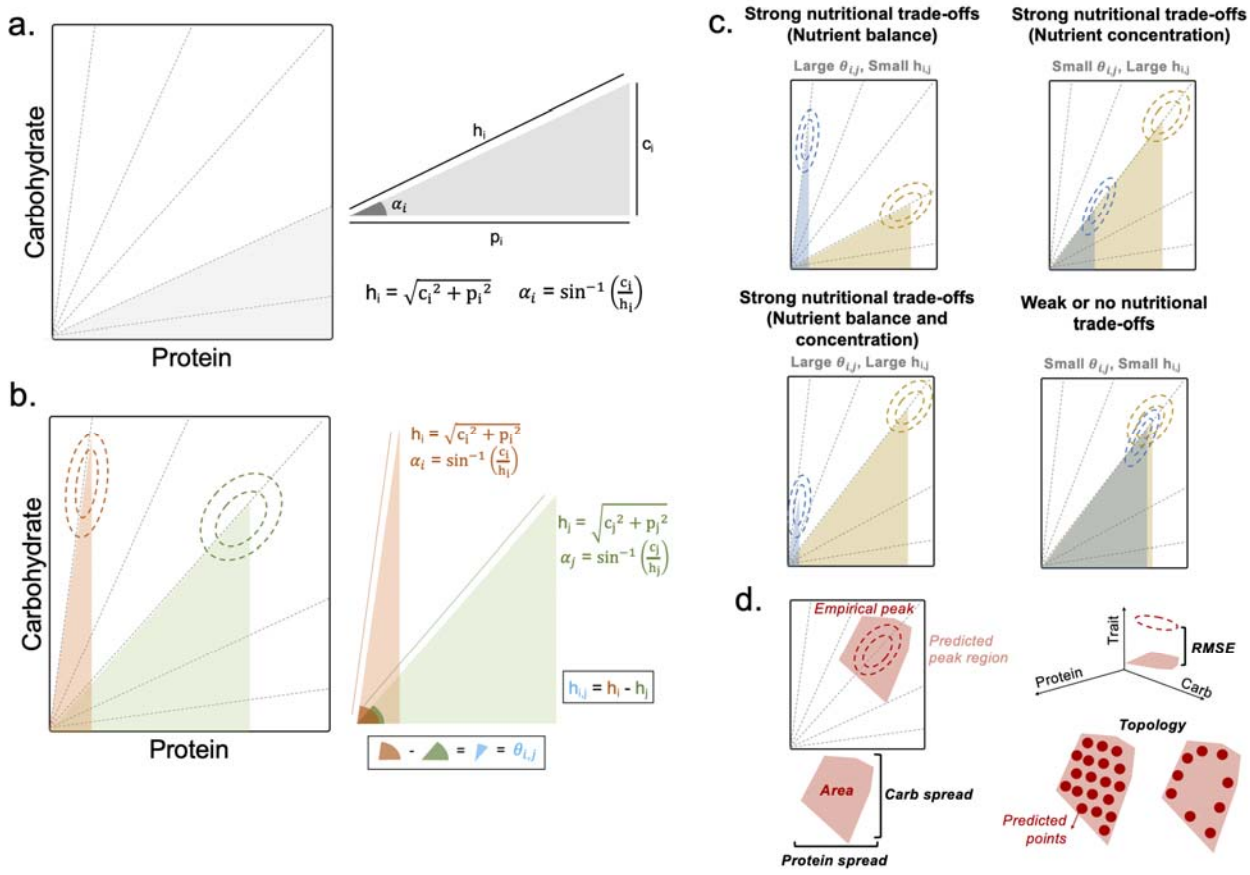

Figure 1. Nutrigonometry framework. (a) Considering an infinite number of nutritional rails that divide the nutritional space into right-angle triangles, the angle and the hypothenuse can be calculated from trigonometric relationships. (b) Nutrigonometry applied to compare two traits is simple as it allows for the estimates of the strength of nutritional trade-offs in terms of nutrient balance (angle) and nutrient concentration (the difference , given in absolute terms). (c) Plausible scenarios for the estimates of and . (d) Metrics used to the peak prediction in the 3D landscape. RMSE was calculated as root-mean-square difference between the predicted and observed values of the trait (z-axis) in the peak region. Nutrient spread (both carbohydrate and protein) was calculated as the standard deviation of the predicted peak region. The area of the polygon that encapsulates the predicted peak region was also estimated as a proxy of prediction performance. Lastly, the topology of the predicted datapoints for the peak region was analysed using the concept of persistence homology (see Methods) to identify homogeneity in predicted point structure.

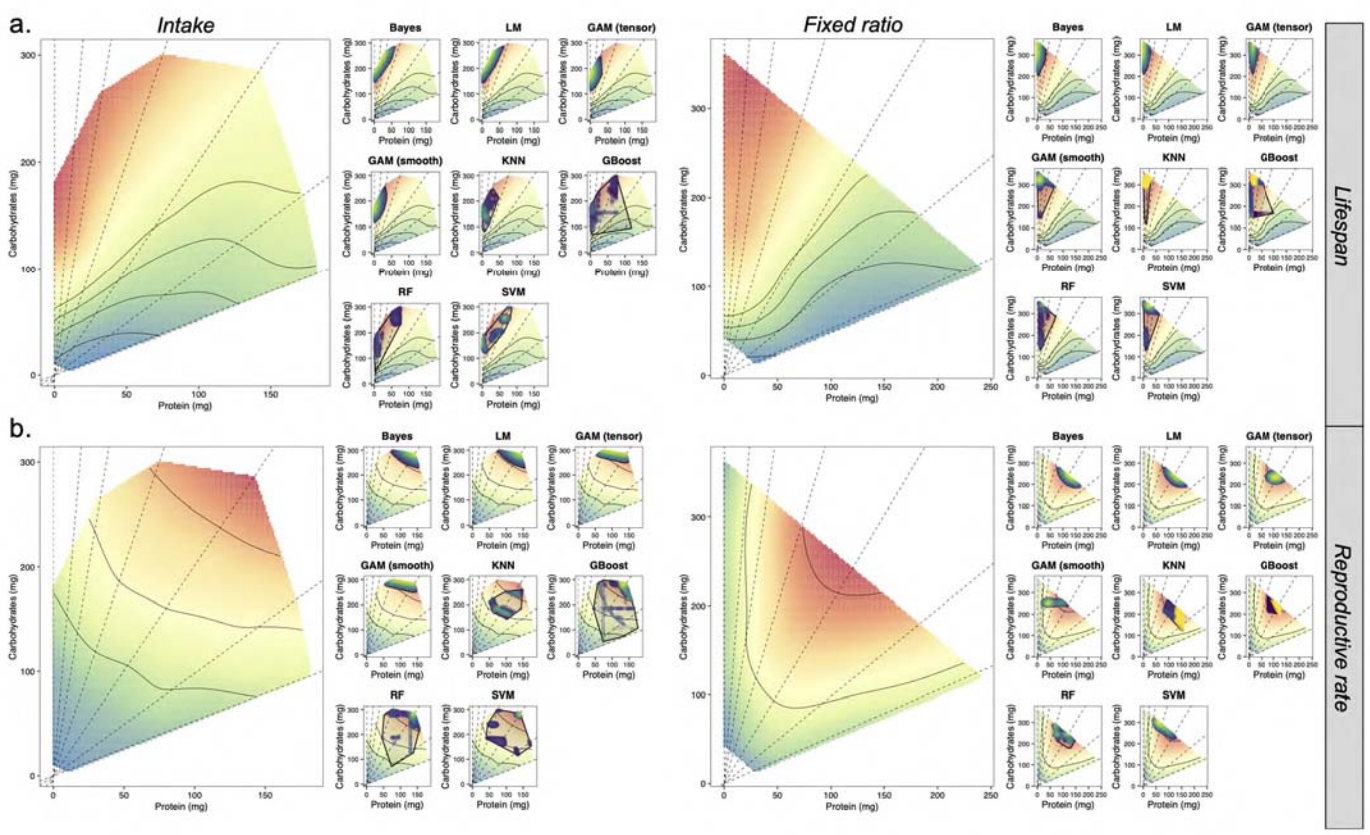

Figure 2. Nutrigonometry framework to predict peak region in lifespan and reproductive rate landscape with different data structure. (a) Lifespan landscapes with individual intake (top left panel) and fixed ratio (top right panel) from Lee et al. (2008) with the overlaid predicted peak regions. (b) Reproductive rate landscapes with individual intake (bottom left panel) and fixed ratio (bottom right panel) from Lee et al. (2008) with the overlaid predicted peak regions. For the landscapes, red represents peaks while light green represents valleys. For the predicted region, dark blue represents points with lower predicted z-values whereas bright yellow represents points with higher predicted z-values. The shaded polygon was added to facilitate visualisation of the predicted peak region and the homogeneity of points within the predicted peak.

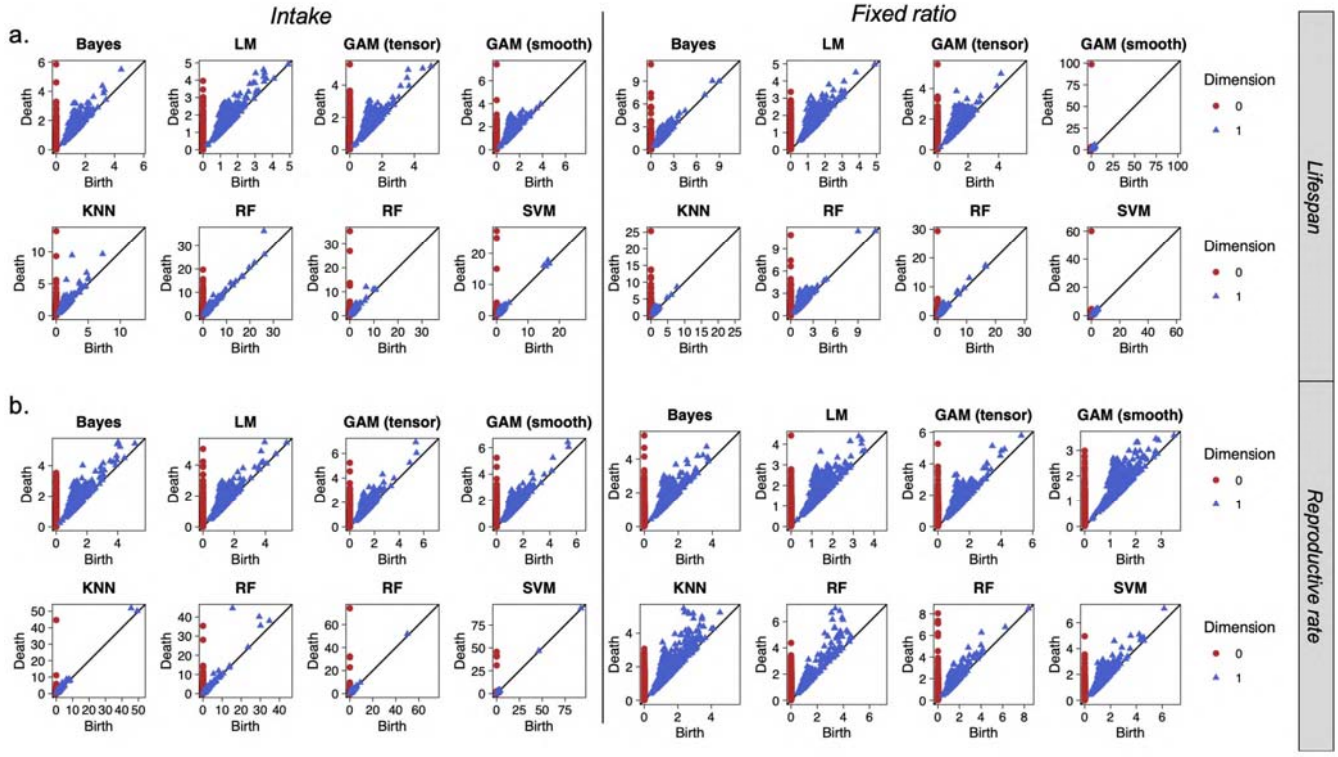

Figure 3. Persistence Homology (PH) to investigate topological structure of the predicted peak region using Nutrigonometry. (a) PH plots for the topological analysis of the predicted peak region in lifespan of data containing the structure of individual intake (top left) and fixed intake data (top right). (b) PH plots for the topological analysis of the predicted peak region in reproductive rate with data of structure containing individual intake (bottom left) and fixed intake data (bottom right). Homogenous predicted peaks have red (dimension 0) and blue (dimension 1) points that are closer, as opposed to more heterogeneous predicted peaks upon which (some) points can be farther from each other. Note the different scales upon which the data is plotted (needed to aid visualisation of point clouds).

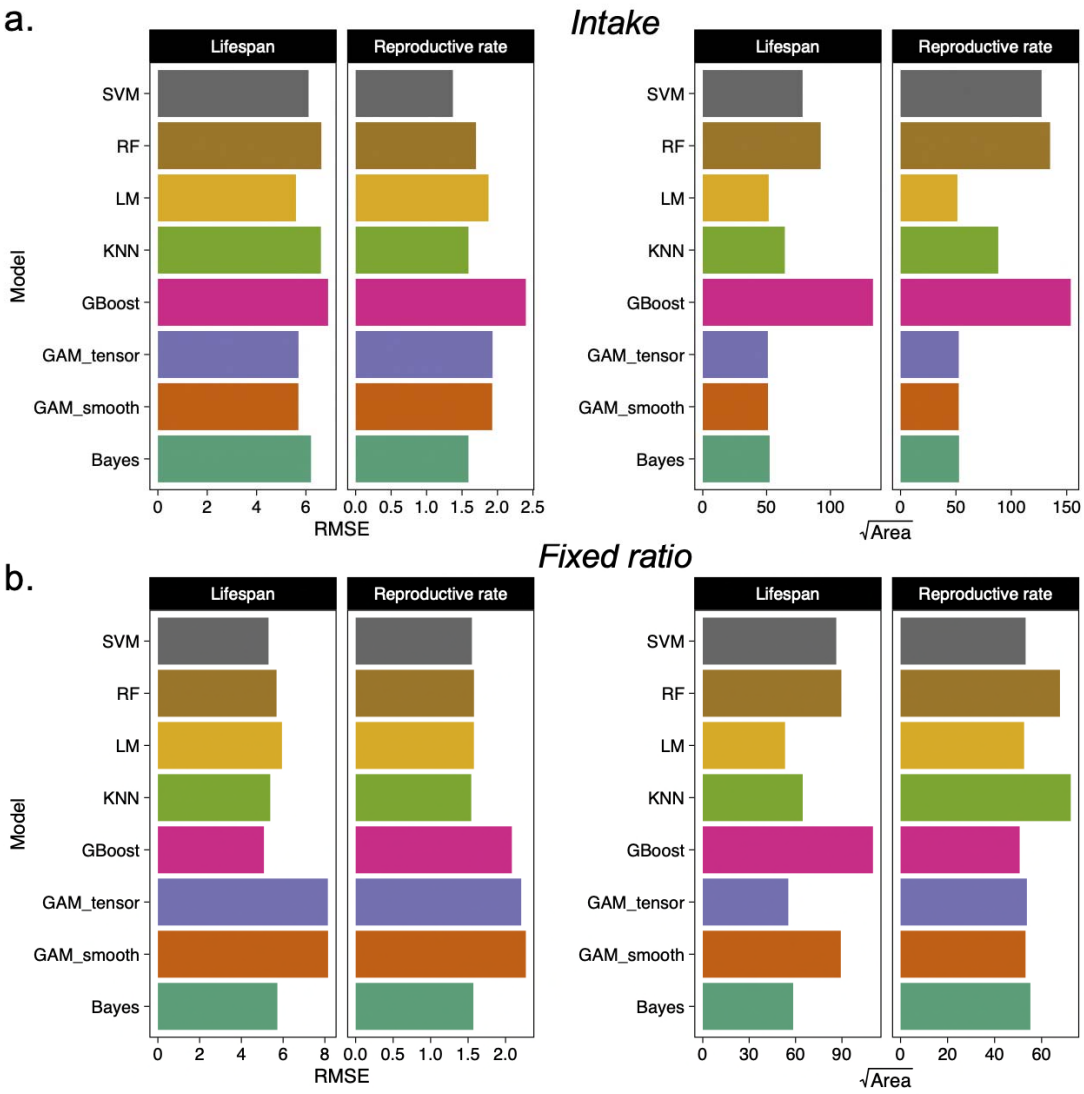

Figure 4. RMSE and peak area estimates in the Nutrigonometry peak region predictions. (a) RMSE and predicted peak area (i.e., area of the shaded polygon from the predicted region for lifespan and reproductive rate data), with structure containing individual intakes. (b) RMSE and predicted peak area (i.e., area of the shaded polygon from the predicted region for lifespan and reproductive rate data), with structure containing fixed ratios. Note that models with high RMSE can still be the best predictors of peak region.

Supplementary Material

Text S1. What is Persistence Homology (PH)? A brief introduction.

Table S1. Area of the predicted peak region for all models. All values are given in unit squared of nutrient intake or diet composition (for fixed ratios).

Table S2. Nutrient spread of the predicted peak region for all models. All values are given in units of nutrient intake or diet composition (for fixed ratios).

Table S3. Nutrigonometry quantification of nutritional trade-offs in developmental time between two developmental temperatures. Estimates of $\theta_{i,j}$ (in degrees) and $h_{i,j}$ (in g/L). Analysis from the data presented in Kutz et al. (2018). Confidence intervals overlapping zero implies no difference in the peaks. Magnitude of the estimates indicate the strength of nutritional trade-offs (i.e., larger magnitudes indicate stronger nutritional trade-offs). Note that $\theta_{i,j}$ is bound between 0 and 90 degrees (i.e., 0 and $\frac{\pi}{2}$).

Figure S1. (a) 3D landscape for developmental time at 25^{o}C (top left) and 28^{o}C (bottom left) (from Kutz et al., 2019) with the overlaid predicted peak regions. For the landscape, red represents peaks while light green represents valleys. For the predicted region, dark blue points represent points with lower predicted z-values whereas bright yellow represents points with higher predicted z-values. The shaded polygon was added to facilitate visualisation of the predicted peak region and the homogeneity of points within the predicted peak. (b) RMSE and predicted peak area (i.e., area of the shaded polygon in panel *a*) for the models of developmental time at 25^{o}C (top right) and 28^{o}C (bottom right) values of each model. Note that models with high RMSE can still be the best predictors of peak region. (c) Persistence homology (PH) plots for the topological analysis of the predicted peak region of the 3D landscape for developmental time at 25^{o}C (top panel) and 28^{o}C (bottom panel) (from Kutz et al., 2019). x and y- axes represent birth and death, respectively, of topological structures. The diagonal line represents the line in which the birth and death co-occur. Homogenous predicted peaks have red (dimension 0) and blue (dimension 1) points that are closer, as opposed to more heterogeneous predicted peaks upon which points are farther from each other**.**

Figure S2. Prediction of the valley regions for lifespan using individual intake data from Lee et al. (2008). Note that we used the best performing models for the peak region (see Main text).

Figure S3. Prediction of the valley regions for reproductive rate using individual intake data from Lee et al. (2008). Note that we used the best performing models for the peak region (see Main text).

R Script. R script with functions for the implementation of the Nutrigonometry framework (separate file).

Table 1. Nutrigonometry quantification of nutritional trade-offs between lifespan and reproduction. Estimates of $\theta_{i,j}$ (in degrees) and $h_{i,j}$ (in mg) for the nutritional trade-off between lifespan and reproductive rate. Analysis from the data presented in Lee et al. (2008). Confidence intervals overlapping zero implies no difference in the peaks. Magnitude of the estimates indicate the strength of nutritional trade-offs (i.e., larger magnitudes indicate stronger nutritional trade-offs). Note that $\theta_{i,j}$ is bound between 0 and 90 degrees (i.e., 0 and $\frac{\pi}{2}$).

	Parameter	Model	Estimate	Std	LwrCI	UprCI
Trade-off (intakes)	$\theta_{i,j}$	**SVM**	14.456	10.728	-6.574	35.485
		RF	14.508	8.109	-1.388	30.404
		GAM_tensor	16.128	4.984	6.358	25.897
		GAM_smooth	16.166	4.962	6.438	25.893
		GBoost	17.063	9.575	-1.706	35.831
		LM	17.940	4.826	8.479	27.400
		Bayes	18.205	4.709	8.974	27.436
		KNN	21.203	6.181	9.088	33.318
	$h_{i,j}$	**SVM**	16.792	65.723	-112.038	145.622
		KNN	50.015	48.137	-44.343	144.373
		GBoost	52.851	75.218	-94.591	200.293
		RF	58.561	66.066	-70.943	188.064
		LM	75.870	35.142	6.984	144.757
		Bayes	76.729	34.444	9.211	144.247
		GAM_smooth	120.245	29.406	62.604	177.886
		GAM_tensor	124.533	27.930	69.784	179.282
Trade-off (fixed)	$\theta_{i,j}$	**GAM_smooth**	9.645	5.897	-1.916	21.205
		SVM	11.840	5.649	0.767	22.913
		RF	17.368	5.848	5.906	28.831
		GBoost	20.177	5.057	10.264	30.090
		GAM_tensor	21.177	3.872	13.588	28.766
		Bayes	26.454	5.876	14.935	37.973
		LM	26.499	5.903	14.928	38.070
		KNN	31.428	7.186	17.342	45.513
	$h_{i,j}$	**SVM**	2.381	68.888	-132.653	137.416
		RF	4.819	64.841	-122.283	131.921
		GBoost	9.377	65.605	-119.222	137.975
		Bayes	41.461	34.912	-26.974	109.896
		LM	42.305	34.429	-25.182	109.791
		GAM_smooth	46.635	40.358	-32.475	125.745
		GAM_tensor	49.009	32.855	-15.394	113.412
		KNN	82.516	30.388	22.949	142.083

Table 2. Nutrigonometry estimates of nutritional compromises. Estimates of optimal intake that maximises lifespan and reproductive rate based on the predicted peak region. Comparison made with the visual peak ratio from Lee et al. (2008). Note that all models show that the estimated peak ratio between traits do not overlap and thus, corroborate the inference of a nutritional trade-off between traits, leading to a nutritional compromise. Note also that all but one model (i.e., GAM smooth for fixed ratio reproductive rate data) predicted peak region ~1:4, which is the ratio that individuals balance when given the ability to balance their diet ('choice'). All other models suggest that a P:C ratio of 1:4 is lower than the ratio needed to maximise lifespan but higher than that for reproductive rate, further supporting the concept of a nutritional compromise.

Data	Trait	Model	Mean	Upr CI	Lwr CI	Target (Visual)
Peak Ratio (intakes)	Lifespan	GBoost	5.235	5.205	5.265	16
		RF	5.533	5.508	5.557	
		SVM	5.864	5.836	5.892	
		LM	9.084	9.048	9.120	
		Bayes	9.154	9.118	9.190	
		KNN	12.075	12.015	12.135	
		GAM_smooth	13.055	12.997	13.114	
		GAM_tensor	13.108	13.049	13.168	
	Reproductive rate	GBoost	1.858	1.853	1.864	2
		KNN	2.041	2.037	2.045	
		RF	2.138	2.133	2.144	
		SVM	2.147	2.138	2.156	
		Bayes	2.194	2.191	2.197	
		LM	2.215	2.212	2.219	
		GAM_smooth	2.644	2.639	2.650	
		GAM_tensor	2.661	2.656	2.667	
Peak Ratio (fixed)	Lifespan	GBoost	13.078	12.987	13.170	16
		SVM	14.946	14.873	15.019	
		RF	15.107	15.045	15.169	
		GAM_smooth	16.977	16.859	17.097	
		GAM_tensor	20.623	20.536	20.710	
		KNN	26.050	25.929	26.173	
		Bayes	32.426	32.237	32.617	
		LM	32.933	32.744	33.125	
	Reproductive rate	KNN	1.467	1.463	1.470	2
		LM	1.836	1.832	1.839	
		Bayes	1.841	1.837	1.845	
		GBoost	2.171	2.168	2.174	
		GAM_tensor	2.244	2.241	2.248	
		RF	2.545	2.539	2.552	
		SVM	3.527	3.516	3.538	
		GAM_smooth	4.280	4.265	4.296	